

Iron(III) benzhydroxamates of dipicolylamines for photocytotoxicity in red light and cellular imaging



Aditya Garai^a, Uttara Basu^a, Imran Khan^b, Ila Pant^b, Akhtar Hussain^a, Paturu Kondaiah^{b,**}, Akhil R. Chakravarty^{a,*}

^a Department of Inorganic and Physical Chemistry, Indian Institute of Science, Sir C.V. Raman Avenue, Bangalore 560012, India

^b Department of Molecular Reproduction and Development Genetics, Indian Institute of Science, Sir C.V. Raman Avenue, Bangalore 560012, India

ARTICLE INFO

Article history:

Received 4 December 2013

Accepted 5 February 2014

Available online 20 February 2014

Keywords:

Iron
Dipicolylamine bases
Hydroxamate
Crystal structure
Photocytotoxicity
Cellular imaging

ABSTRACT

Benzhydroxamate (BHA) iron(III) complexes [Fe(BHA)(L)Cl]Cl (**1**, **2**), where L is (phenyl)dipicolylamine (phdpa in **1**) and (pyrenyl)dipicolylamine (pydpa in **2**), were prepared and their photocytotoxicity in visible (400–700 nm) and red (600–720 nm) light was studied. Complex **1** was structurally characterized by X-ray crystallography. The complexes have high-spin iron(III) centers. Complex **2**, with a pyrenyl fluorophore, was used for cellular imaging, showing both mitochondrial and nuclear localization in the fluorescence microscopic study. The complex exhibited photocytotoxicity in red light in HeLa cancer cells, giving IC₅₀ value of 24.4(±0.4) μM, but remained essentially non-toxic in the dark. The involvement of reactive oxygen species and an apoptotic nature of cell death were observed from the cellular studies.

© 2014 Elsevier Ltd. All rights reserved.

1. Introduction

Photodynamic therapy (PDT) is a non-invasive method for the treatment of cancer in which an administered drug, on photo-activation at the cancer site, generates a reactive oxygen species (ROS) which selectively damages only the photo-exposed cancer cells, leaving the unexposed healthy cells unaffected [1–7]. Macrocyclic organic dyes based on porphyrin, phthalocyanine and related compounds have been extensively studied as potential PDT agents with Photofrin[®] having FDA approval as a PDT drug. These compounds generate singlet oxygen (¹O₂) as the ROS via a type-II energy transfer pathway. The efficacy of such organic dyes thus largely depends upon their ability to generate ¹O₂ in the cancer cells [8]. The drawbacks associated with Photofrin[®] are prolonged skin sensitivity and hepatotoxicity due to formation of bilirubin as a breakdown product of the drug, thus limiting its therapeutic potential [9,10]. An alternate and useful approach to circumvent these predicaments could be designing and synthesizing redox active metal-based PDT agents that are capable of showing similar therapeutic effects in red light through type-I and/or photo-redox pathways generating ROS [11]. Biocompatible 3d-metal

complexes, with their versatile coordination geometries, varied spectral and redox properties, could be suitably designed to achieve the basic requirements of PDT. While several metal complexes have been studied earlier for their PDT activity, the potential of iron complexes in PDT remains virtually unexplored [12–20]. The present work stems from our interest to develop the chemistry of iron-based PDT agents. There are a few notable recent developments in the chemistry of metal-based photocytotoxic agents. Sadler and co-workers have reported a six-coordinate platinum(IV) complex as a photo-activated metallo-drug with two *trans*-azide ligands, which is stable in the dark, but generates a *trans*-(diguandine)-platinum(II) adduct on photoactivation, showing cytotoxicity [12,13]. Photocytotoxic nitrosyl ruthenium complexes are reported for site-specific delivery of nitric oxide (NO) on exposure to visible light [14]. Dirhodium(II) complexes have been shown to cause oxidative DNA damage in visible light through both oxygen-dependent and independent pathways [15]. We have reported the photocytotoxicity of copper(II) and oxovanadium(IV) complexes in visible light [16–19]. Although oxovanadium(IV) complexes show low dark cytotoxicity, the low molar extinction coefficient (ϵ) values of their d–d band near 700 nm make them less effective as near-IR light photosensitizers. Copper(II) complexes are generally unsuitable as PDT agents due to their high dark cytotoxicity, resulting from the reduction of the metal by glutathione and other cellular thiols generating radical species [21,22].

* Corresponding author. Tel.: +91 80 2293 2533; fax: +91 80 2360 0683.

E-mail addresses: paturu@mrdg.iisc.ernet.in (P. Kondaiah), arc@ipc.iisc.ernet.in (A.R. Chakravarty).

** Fax: +91 80 23600999.

We have now designed some new iron(III) complexes having the naturally occurring chelating biocompatible hydroxamate ligand and dipicolylamine with a pendant planar pyrenyl moiety as a fluorophore. Iron is an essential bio-element and its complexes, showing significant PDT activity in visible light, could have better therapeutic utility [20]. Herein, we report the synthesis, structure and visible light-induced cytotoxicity of two benzhydroxamate (BHA) iron(III) complexes, viz. $[\text{Fe}(\text{BHA})(\text{L})\text{Cl}]\text{Cl}$ (**1**, **2**) where L is (phenyl)dipicolylamine (phdpa in **1**) and (pyrenyl)dipicolylamine (pydpa in **2**) (Fig. 1). A significant result of this study is the observation of mitochondrial localization of the pyrenyl complex **2** from fluorescence microscopy. Photofrin[®] is also known to localize in the mitochondria for drug action. With the intrinsic pathway of apoptosis largely depending on the mitochondria, targeting this cellular organelle with a suitably designed compound could result in desirable photo-induced cytotoxicity [23–25]. Mitochondria targeting anticancer agents are likely to overcome the resistance mechanism in the conventional chemotherapeutic drug action, thus increasing the potential of the PDT drug. Complex **2** also showed a remarkable photocytotoxic effect in HeLa cancer cells in visible light of 400–700 nm and red light of 600–720 nm, while remaining essentially non-toxic in the dark.

2. Experimental

2.1. Materials and methods

All reagents and chemicals were purchased from commercial sources (S.D. Fine Chemicals, India; Aldrich-Sigma, USA; Invitrogen Bio Services, India) and were used without further purification. Supercoiled pUC19 DNA (CsCl purified) was procured from Bangalore Genie (India). Calf thymus (ct) DNA, agarose (molecular biology grade), distamycin, methyl green, catalase, SOD and ethidium bromide were obtained from Sigma (USA). Tris-(hydroxymethyl)aminomethane-HCl (Tris-HCl) buffer was prepared using deionised and sonicated triple distilled water. The solvents used for the synthesis, electrochemical and spectral measurements were purified by conventional procedures. The dipicolylamine derivatives, viz. N-benzyl-1-(pyridin-2-yl)-N-[(pyridin-2-yl)methyl]-methanamine (phdpa) and N-[(pyren-1-yl)methyl]-1-(pyridin-2-yl)-N-[(pyridin-2-yl)methyl]-methanamine (pydpa) were prepared following literature methods [26,27].

The elemental analyses were performed with a Thermo Finnigan FLASH EA 1112 CHNS analyzer. The infrared, absorption and emission spectra were recorded with Perkin-Elmer Lambda 35, Perkin-Elmer Lambda 650 and Perkin-Elmer LS 55 spectrophotometers, respectively, at 25 °C. Molar conductivity measurements were done with a Control Dynamics (India) conductivity meter. Electrochemical measurements were made at 25 °C with an EG&G PAR model 253 VersaStat potentiostat/galvanostat with electrochemical analysis software 270, using a three-electrode setup consisting of a glassy carbon working, platinum wire auxiliary and a saturated calomel reference electrode (SCE).

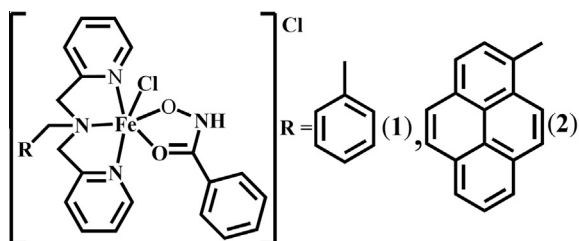


Fig. 1. Schematic drawings of the complexes **1** and **2**.

Tetrabutylammonium perchlorate (TBAP, 0.1 M) was used as a supporting electrolyte for the electrochemical measurements. ESI-MS measurements were carried out with a Bruker Daltonics make Esquire 300Plus ESI model. Flow cytometric analysis was performed with a FACS Calibur (Becton Dickinson (BD)) cell analyzer at the FL2 channel (595 nm). Fluorescence microscopy images were recorded with Olympus IX 81 microscope. Cellular uptake measurements were performed with an inductively coupled plasma optical emission spectrometer, Perkin-Elmer ICP-OES (Model Optima 2000 DV).

2.2. Preparation of $[\text{Fe}(\text{BHA})(\text{L})\text{Cl}]\text{Cl}$ ($L = \text{phdpa}$, **1**; pydpa , **2**)

To a methanolic solution of ferric chloride (0.16 g, 1.0 mmol) was added the dipicolylamine base (L, 0.29 g for **1** and 0.41 g for **2**, 1.0 mmol) dissolved in methanol, and the solution was stirred for 30 min to get a precipitate of the precursor complex $[\text{Fe}(\text{L})\text{Cl}_3]$, which was filtered and air dried [Yield: for **1**, 0.39 g (~85%); for **2**, 0.52 g (~90%)]. To the suspension of the precursor complex (L, 0.45 g for **1** and 0.57 g for **2**, 1.0 mmol) was added dropwise a solution of benzhydroxamic acid (0.14 g, 1.0 mmol) and triethylamine (0.10 g, 1.0 mmol), also in methanol, to give a deep purple colored solution, which on slow evaporation of the solvent gave a solid that was isolated, washed with diethyl ether and finally dried in a vacuum over P_4O_{10} .

$[\text{Fe}(\text{BHA})(\text{phdpa})\text{Cl}]\text{Cl}\cdot\text{H}_2\text{O}$ (**1**· H_2O): Yield: 0.42 g (~75%). Anal. Calc. for $\text{C}_{26}\text{H}_{27}\text{Cl}_2\text{FeN}_4\text{O}_3$ (MW: 570.27): C, 54.76; H, 4.77; N, 9.82. Found: C, 54.49; H, 5.07; N, 9.53%. ESI-MS in MeOH, m/z : 512.17 $[\text{M}-2\text{Cl}^- + \text{MeO}^-]^+$, 480.52 $[\text{M}-2\text{Cl}^- - \text{H}^+]^+$. IR (solid phase, cm^{-1}): 3397 (br), 2944 (m), 2600 (m), 2490 (m), 1604 (s), 1480 (s), 1438 (s), 1345 (m), 1150 (s), 1026 (s), 913 (s), 810 (s), 760 (s), 706 (s), 540 (w), 479 (w) (br, broad; s, strong; m, medium; w, weak). UV-Vis (DMF) λ_{max} , nm (ϵ , $\text{M}^{-1}\text{cm}^{-1}$): 454 (1420), 268 (6380). Molar conductance in DMF at 25 °C: $\Lambda_{\text{M}} = 67\text{ S m}^2\text{ M}^{-1}$. $\mu_{\text{eff}} = 5.85\ \mu_{\text{B}}$ at 298 K.

$[\text{Fe}(\text{BHA})(\text{pydpa})\text{Cl}]\text{Cl}\cdot\text{H}_2\text{O}$ (**2**· H_2O): Yield: 0.54 g (~79%). Anal. Calc. for $\text{C}_{36}\text{H}_{31}\text{Cl}_2\text{FeN}_4\text{O}_3$ (MW: 694.41): C, 62.27; H, 4.50; N, 8.07. Found: C, 62.50; H, 4.76; N, 8.21%. ESI-MS in MeOH, m/z : 636.27 $[\text{M}-2\text{Cl}^- + \text{MeO}^-]^+$, 604.47 $[\text{M}-2\text{Cl}^- - \text{H}^+]^+$, 640.07 $[\text{M}-\text{Cl}^-]^+$. IR (solid phase, cm^{-1}): 3377 (br), 2933 (m), 2666 (m), 1603 (s), 1490 (s), 1448 (s), 1345 (m), 1140 (m), 1070 (m), 1030 (m), 913 (m), 850 (s), 768 (s), 685 (s), 553 (w), 490 (w). UV-Vis (DMF) λ_{max} , nm (ϵ , $\text{M}^{-1}\text{cm}^{-1}$): 466 (1530), 345 (22,100), 328 (15,800), 315 (8340), 277 (24,190), 267 (18,480). Molar conductance in DMF at 25 °C: $\Lambda_{\text{M}} = 72\text{ S m}^2\text{ M}^{-1}$. $\mu_{\text{eff}} = 5.88\ \mu_{\text{B}}$ at 298 K.

2.3. X-ray crystallographic procedure

The crystal structure of $[\text{Fe}(\text{BHA})(\text{phdpa})\text{Cl}]\text{Cl}\cdot\text{H}_2\text{O}$ (**1**· H_2O) was obtained by the single crystal X-ray diffraction method. Crystals of the composition **1**· H_2O were isolated from a methanol solution of the complex on slow evaporation. Crystal mounting was done on a glass fibre with epoxy cement. All geometric and intensity data were collected at room temperature using an automated Bruker SMART APEX CCD diffractometer equipped with a fine-focus 1.75 kW sealed-tube Mo $\text{K}\alpha$ X-ray source ($\lambda = 0.71073\ \text{\AA}$) with increasing ω (width of 0.3° per frame) at a scan speed of 5 s per frame. Intensity data, collected using the $\omega-2\theta$ scan mode, were corrected for Lorentz-polarization effects and for absorption [28]. The structure solution was done by a combination of Patterson and Fourier techniques and refined by full-matrix least-squares methods using the SHELX system of programs [29]. Hydrogen atoms of the complex were placed in their calculated positions and refined using a riding model. The non-hydrogen atoms were refined anisotropically. A molecular view was obtained using ORTEP [30].

2.4. Cell cytotoxicity

The photocytotoxicity of the complexes was assessed by an MTT assay [31]. Approximately 8000 HeLa cells were plated in a 96-well culture plate in Dulbecco's Modified Eagle Medium (DMEM) supplemented with 10% fetal bovine serum (FBS) [32]. After 24 h of incubation at 37 °C, different concentrations of the complexes **1** and **2** were added to the cells and incubation was continued in the dark for 4 h. After incubation, the medium was replaced with phosphate buffer saline (DPBS) and irradiation was done in visible light, 400–700 nm, using a Luzchem photoreactor (model LZC-1, Ontario, Canada; light fluence rate = 2.4 mW cm⁻²; light dose = 10 J cm⁻²) or a 600–720 nm red light source (Waldmann PDT 1200 L, 100 J cm⁻²). DPBS was replaced with 10% FBS/DMEM after photo-irradiation. Incubation was done in dark for 20 h, following which 20 µL of 5 mg ml⁻¹ MTT was added to each well and incubated for an additional 3 h. The culture medium was discarded and 200 µL of DMSO was added to dissolve the formazan crystals. The absorbance at 540 nm was determined using a Molecular Devices Spectra Max M5 plate reader. The cytotoxicity of the test compounds was measured as the percentage ratio of the absorbance of the treated cells over the untreated controls. The IC₅₀ values were determined by non-linear regression analysis (GraphPad Prism 5).

2.5. DNA Fragmentation analysis

Briefly, 0.3 × 10⁶ cells were taken in each 60 mm dish, grown for 24 h and later treated with the complex (20 µM) for 10 h in the dark. One of the dishes was exposed to visible light (400–700 nm, 10 J cm⁻²) for 1 h and the cells were left to grow for 4 h along with its dark control. The cells were trypsinized, washed with DPBS and re-suspended in 0.4 ml of lysis buffer (10 mM Tris–HCl; pH 8.0, 20 mM EDTA, 0.2% triton-X 100) with an incubation of 20 min on ice. Lysed cells were centrifuged for 20 min at 13000 rpm and their supernatant was collected. Phenol/chloroform treatment was performed to remove the protein present. Later, the supernatant was precipitated with 1/10 volume of 3 M sodium acetate (pH 5.8) and 2 volumes of ethanol at –20 °C overnight. The DNA pellet was washed with 70% alcohol and re-suspended in TE containing RNase (1X Tris–EDTA with 100 µg ml⁻¹ RNase). DNA samples were placed into the well of 1.5% agarose gel. The agarose gels were run at 70 V for ~2 h and photographed under UV light.

2.6. DCFDA assay

The dihydro-analogue of the fluorescent probe 2',7'-dichlorofluorescein diacetate (DCFDA) was used to detect any generation of cellular ROS by flow cytometric analysis. Cell permeable DCFDA on oxidation by ROS generates fluorescent DCF, having an emission maximum at 528 nm [33]. HeLa cancer cells were incubated with the complex (20 µM) for 4 h followed by photo-irradiation (400–700 nm) for 30 min in serum free conditions. The cells were harvested by trypsinization and a single cell suspension of 1 × 10⁶ cells ml⁻¹ was made. The cells were treated with 1.0 µM DCFDA solution in DMSO in the dark for ~15 min. The distribution of DCFDA stained HeLa cells was determined by flow cytometry.

2.7. Fluorescence microscopy using propidium iodide and MitoTracker Red

Uptake of the fluorescent complex **2** into the HeLa cells was studied using a fluorescence microscope. HeLa cells were grown on glass cover slips in each 12-well plates at a seeding density of 5.0 × 10⁴ cells in 1.5 ml of the culture medium for 24 h. The cells

were subsequently treated with the complex for 2 and 4 h in the dark. The cells were then fixed and permeabilized with methanol for 10 min at –20 °C. Methanol was removed, the cells were washed with 1X PBS and incubated with propidium iodide (PI, 10 mg ml⁻¹, diluted to 1:4) to stain the nucleus for 2 min and visualized under a fluorescence microscope. MitoTracker[®] deep red, having a mildly thiol-reactive chloromethyl moiety, was used for labeling the mitochondria. DMEM containing 5 nM of MitoTracker[®] Deep Red FM (M22426) was used for 20 min. The cells after incubation were processed for live cell imaging and were visualized under a fluorescence microscope.

2.8. Cellular uptake measurements

Complexes **1** and **2** (20 µM) in DMSO were added to the cells, giving a final DMSO concentration of 1% v/v. The cells were then incubated for 4 h at 37 °C in a CO₂ incubator. The culture medium was subsequently discarded and the cells were washed thrice with ice cold DPBS of pH 7.4, harvested and taken up in DPBS, followed by centrifugation for 10 min at 3000 rpm at 4 °C. The resulting pellet, after discarding DPBS, was dissolved in 70% nitric acid at 65 °C for 2 h. The samples were diluted to final a 5% nitric acid concentration with water containing 0.1% Triton-X. The iron content of the samples was determined using inductively coupled plasma optical emission spectrometry (ICP-OES) at the emission wavelengths of 238.204 and 239.562 nm for iron. The protein content was estimated after lysing the cell pellet, obtained by a similar treatment of HeLa cells with the complexes, followed by isolation by scraping with 1.0 N NaOH. The total iron content was expressed as the quantity of iron in ng per mg protein.

2.9. DNA binding and cleavage experiments

DNA binding experiments were done in Tris–HCl buffer (5 mM, pH 7.2) using a DMF solution of complexes **1** and **2** using reported procedures [34]. Calf thymus DNA (ca. 250 µM NP) was used for the binding studies [35,36]. The intrinsic equilibrium binding constant (K_b) of **1** and **2** to ct-DNA was obtained by the McGhee–von Hippel (MvH) method using the expression of Bard et al. by monitoring the change of the absorption intensity of the spectral band with increasing concentrations of ct-DNA [37]. Viscosity measurements were made using a Schott Gerate AVS 310 automated viscometer attached to a constant temperature bath at 37 °C. The ct-DNA stock solution was 140 µM (NP, nucleotide pair) in 5 mM Tris–HCl buffer. The complex was added gradually, increasing the concentration from 0 to 120 µM, and the viscosity was measured after each addition. The relative specific viscosity of DNA, $(\eta/\eta_0)^{1/3}$ was plotted vs. [complex]/[DNA], where η is the viscosity of DNA in the presence of the complex and η_0 is the viscosity of ct-DNA alone in 5 mM Tris buffer medium. The viscosity values were calculated from the observed flow time of ct-DNA containing solutions (t), duly corrected for that of the buffer alone (t_0), $\eta = (t-t_0)/t_0$. DNA thermal denaturation studies were done by monitoring the absorption intensity of ct-DNA (150 µM) at 260 nm by varying the temperature from 40 to 90 °C in both the absence and presence of the complexes (10 µM) using a Perkin–Elmer Lambda 650 spectrometer with a temperature controller at an increase rate of 1 °C min⁻¹ for the solution.

The cleavage of SC pUC19 DNA (0.2 µg, 30 µM, 2686 base-pairs) was studied by agarose gel electrophoresis using the complexes in 50 mM Tris–HCl buffer (pH 7.2) and 50 mM NaCl containing 10% DMF in red light of 647 nm using an Ar–Kr mixed gas ion laser of Spectra Physics with a laser power 100 mW [38]. Mechanistic studies were carried out using different additives. The extent of SC DNA cleavage was measured from the intensities of the bands using the UVITEC Gel Documentation System. Necessary corrections were

made for the low level of the nicked circular (NC) form of DNA present in the original SC DNA sample and for the low affinity of ethidium bromide (EB) binding to SC compared to the NC form of DNA [39]. The observed error in measuring the band intensities was ca. 5%.

3. Results and discussion

3.1. Synthesis and general properties

The iron(III) complexes [Fe(BHA)(L)Cl]Cl (**1**, **2**) were prepared by reacting a methanol solution of the dipicolylamine derivative (L) with FeCl₃ to obtain a precursor complex which on further treatment with benzhydroxamic acid (HBHA) and triethylamine in methanol formed the complexes in high yield [26,27,40]. The complexes were characterized from their analytical and physicochemical data (Table 1). The ESI-MS of the complexes in methanol showed a prominent peak corresponding to the species [M–2Cl[−]+MeO[−]]⁺ along with the [M–2Cl[−]–H⁺]⁺ peak of lower relative abundance, suggesting substitution of the chloride ligand by a methoxy (MeO[−]) group from the solvent. The complexes are 1:1 electrolytes in DMF, giving a molar conductivity (Λ_M) value of $\sim 70 \text{ S m}^2 \text{ M}^{-1}$. The electronic absorption spectra of the complexes in DMF showed a broad and intense band near 470 nm with a tail that extends up to 650 nm (Fig. 2). The spectral peaks in the UV region are due to π – π^* transitions involving the ligands [41]. The low energy visible band is assignable to the benzhydroxamate to iron(III) ligand-to-metal charge transfer (LMCT) transition, involving the frontier orbital of the hydroxamate and the $d\pi^*$ orbital of iron(III) [40]. Complex **2** showed an emission band at 394 nm upon excitation at 347 nm, giving a quantum yield (ϕ) value of 0.08 in DMSO (Fig. 2). The pydpa ligand alone gave a ϕ value of 0.12 under similar experimental conditions. The IR spectra of the complexes displayed a strong peak at 1600 cm^{-1} and a weak peak at 3380 cm^{-1} corresponding to the C=O and N–H stretching vibrations of BHA [42]. The complexes gave a room temperature magnetic moment value of $\sim 5.85 \mu_B$, indicating the high-spin nature of iron(III). Cyclic voltammetry of the complexes showed a quasi-reversible Fe(III)–Fe(II) redox couple near 0.1 V vs. SCE in DMF/0.1 M TBAP. Addition of 3-mercaptopropionic acid as a reducing agent to a solution of complex **2** showed a gradual decrease in the UV–Vis spectral peak absorbance with a concomitant increase in the intensity of a new peak assignable to the formation of the corresponding iron(II) species.

Table 1
Selected physicochemical and ct-DNA binding data of complexes **1** and **2**.

	1	2
IR ^a /cm ^{−1} [$\bar{\nu}$ (C=O)]	1604	1603
Electronic ^b : λ_{max} /nm ($\epsilon/\text{M}^{-1} \text{ cm}^{-1}$)	454 (1420)	466 (1530)
Emission ^c [λ_{em} /nm]	–	394
μ_{eff} ^d	5.85	5.88
Λ_M ^e /S m ² M ^{−1}	67	72
E_f^f /V(ΔE_p /mV)	0.054 (316)	0.079 (191)
K_b^g /M ^{−1}	$(2.6 \pm 0.5) \times 10^5$	$(6.4 \pm 0.8) \times 10^5$
ΔT_m^h /°C	1.0	4.0

^a In KBr phase.

^b Visible electronic spectral band in DMF.

^c Emission peak of **2** in DMSO with λ_{ex} of 347 nm.

^d Magnetic moment (μ_{eff}) in μ_B obtained by the ¹H NMR method at 298 K.

^e Λ_M , molar conductance in DMF at 25 °C.

^f Fe(III)–Fe(II) redox couple in DMF/0.1 M TBAP at 50 mV s^{−1} scan rate.

^g Equilibrium DNA binding constant determined from the UV–Vis absorption titration.

^h Change in the DNA melting temperature after addition of the complexes.

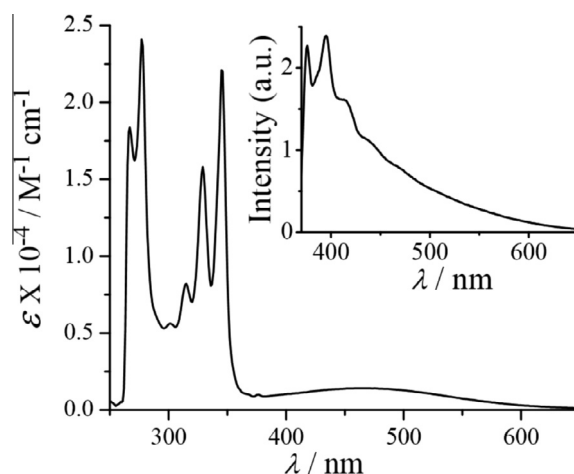


Fig. 2. UV–Vis spectrum of complex **2** in DMF with the inset showing the emission spectrum of **2** in DMSO ($\lambda_{\text{ex}} = 347 \text{ nm}$).

3.2. X-ray crystallography

Complex **1**, as a monohydrate, was structurally characterized by single-crystal X-ray crystallography. It crystallized in the $P2_1/n$ space group of the monoclinic crystal system [29]. An ORTEP view of the cationic complex is shown in Fig. 3 [30]. Selected crystallographic data and important bond distance and bond angle data are given in Tables 2 and 3, respectively. The structure shows the iron is in a six coordinate {Fe^{III}N₃O₂Cl} geometry with the metal bonded to the tridentate *N,N,N*-donor (phenyl)dipicolylamine ligand in a meridional mode of bonding, the bidentate *O,O*-donor mono-anionic BHA and a monodentate chloride ligand [20]. The Fe(1)–N(2) bond is longer than the other two Fe–N distances due to the sp^3 hybridization of the N(2) atom. The Fe–O distances are ~ 2.0 Å. The Fe–Cl bond distance is 2.2649(8) Å. The coordination geometry is significantly distorted from an ideal octahedron. The N(1)–Fe(1)–N(3) bond angle is 150.67(8)°. The O(2)–Fe(1)–N(2) angle shows $\sim 11^\circ$ deviation from the expected *trans* disposition.

3.3. Solubility and stability

The complexes showed good solubility in common organic solvents like methanol, ethanol, DMF, DMSO and acetonitrile, and were moderately soluble in water. They were insoluble in hydrocarbon solvents. A study on the solution stability of the complexes

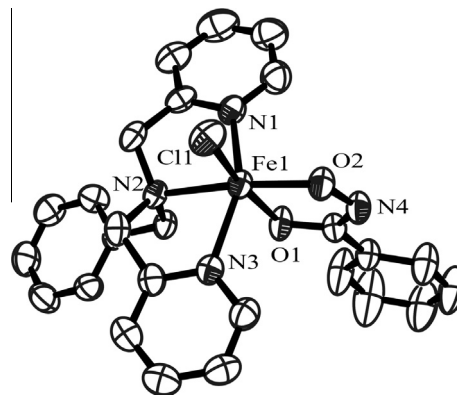


Fig. 3. An ORTEP view of the cationic species in [Fe(BHA)(phdpa)Cl]Cl·H₂O (**1**·H₂O) showing the atom numbering scheme for the metal and hetero-atoms. The hydrogen atoms are omitted for clarity.

Table 2
Selected crystallographic data for [Fe(BHA)(phdpa)Cl]Cl·H₂O (1·H₂O).

Empirical formula	C ₂₆ H ₂₇ Cl ₂ Fe N ₄ O ₃
Formula weight (g M ⁻¹)	570.27
Crystal system	monoclinic
Space group	<i>P2₁/n</i>
<i>a</i> (Å)	8.8604 (8)
<i>b</i> (Å)	14.5967 (14)
<i>c</i> (Å)	20.670 (2)
$\alpha = \gamma$ (°)	90.00
β (°)	99.731 (6)
<i>V</i> (Å ³)	2634.8 (4)
<i>Z</i>	4
<i>T</i> (K)	293 (2)
ρ_{calc} (g cm ⁻³)	1.438
λ (Å) (Mo K α)	0.71073
μ (mm ⁻¹)	0.810
Data/restraints/parameters	4631/0/329
<i>F</i> (000)	1180
Goodness-of-fit (GOF)	1.027
$R(F_o)^a, I > 2\sigma(I)$ [$wR(F_o)$] ^b	0.0367 [0.0846]
R (all data) [wR (all data)]	0.0575 [0.0918]
Largest difference in peak and hole (e Å ⁻³)	0.271, -0.249

^a $R = \sum ||F_o| - |F_c|| / \sum |F_o|$.
^b $wR = \{ \sum [w(F_o^2 - F_c^2)^2] / \sum [w(F_o)^2] \}^{1/2}$. $w = [\sigma^2 F_o^2 + (AP)^2 + BP]^{-1}$, where $P = (F_o^2 + 2F_c^2)/3$, $A = 0.0433$; $B = 0.7893$.

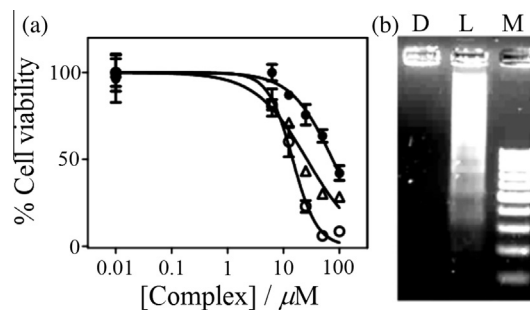
Table 3
Selected bond distances (Å) and bond angles (°) for [Fe(BHA)(phdpa)Cl]Cl·H₂O (1·H₂O).

Fe(1)–O(1)	2.0596(17)	O(2)–Fe(1)–N(2)	168.88(7)
Fe(1)–O(2)	1.9230(16)	O(2)–Fe(1)–N(3)	103.10(8)
Fe(1)–N(1)	2.132(2)	O(1)–Fe(1)–Cl(1)	170.49(5)
Fe(1)–N(2)	2.2345(19)	O(2)–Fe(1)–Cl(1)	92.67(5)
Fe(1)–N(3)	2.130(2)	N(1)–Fe(1)–N(2)	75.50(8)
Fe(1)–Cl(1)	2.2649(8)	N(1)–Fe(1)–N(3)	150.67(8)
O(1)–Fe(1)–O(2)	77.83(7)	N(2)–Fe(1)–N(3)	75.53(7)
O(1)–Fe(1)–N(1)	88.26(8)	N(1)–Fe(1)–Cl(1)	94.53(6)
O(1)–Fe(1)–N(2)	91.07(7)	N(2)–Fe(1)–Cl(1)	98.43(5)
O(1)–Fe(1)–N(3)	87.79(8)	N(3)–Fe(1)–Cl(1)	94.12(6)
O(2)–Fe(1)–N(1)	104.42(8)		

was done by UV–Vis spectroscopy in 50% aqueous DMSO. No significant change was observed in the spectra even after 24 h, suggesting that the complexes are generally stable in an aqueous medium, making them suitable for cellular studies.

3.4. Photocytotoxicity

The cytotoxicity of the complexes was assessed in visible light, 400–700 nm (10 J cm⁻²), and red light, 600–720 nm (100 J cm⁻²), using human cervical HeLa cancer cells by an MTT assay. HeLa was chosen as a commonly used cancer cell for our study. The complexes were essentially non-toxic in the dark, giving IC₅₀ values of >75 μM. Complex **2** showed significant photocytotoxicity giving IC₅₀ values of 14.6 ± 0.7 μM in visible light, 400–700 nm, and 24.4 ± 0.4 μM in red light, 600–720 nm (Fig 4(a)). Complex **1** did not show any significant photocytotoxicity. The pydpa ligand alone gave an IC₅₀ value of >100 μM. The photocytotoxicity of complex **2** could be due to the presence of the photo-active pyrene moiety. A comparison of the IC₅₀ values of the present and related complexes is made in Table 4 [20,43,44]. The fragmentation pattern of genomic DNA was studied using HeLa cells to get an insight into the mode of light-induced cell death by the complex. A 20 μM solution of **2** on exposure to visible light, 400–700 nm, showed the formation of a DNA ladder, indicating an apoptotic mode of cell death (Fig 4(b)). No such ladder was observed in the dark suggesting the non-toxic nature of the complex in the absence of light.

**Fig. 4.** (A) Photocytotoxicity of complex **2** in HeLa cells after 4 h incubation in the dark (black circle) and after irradiation with visible light of 400–700 nm (10 J cm⁻², open circle) and red light of 600–720 nm (100 J cm⁻², open triangle). (b) DNA ladder formation induced by **2** upon light exposure in HeLa cells, indicating an apoptotic mode of cell death (D: dark, L: light, M: Marker 100 bp).**Table 4**

The IC₅₀ and iron uptake values for **1** and **2** in HeLa cells along with the IC₅₀ values of some related compounds.

Complex	IC ₅₀ (μM) in light (400–700 nm)	IC ₅₀ (μM) in the dark	Iron uptake (ng mg ⁻¹ of protein) ^a
1 ^b	75.9 ± 0.8 ^c	>100	1.97
2 ^b	14.6 ± 0.7 ^c	77.0	2.79
[Fe(phqpy)] ^{2+ d}	4.3 ± 0.2	7.7 ± 0.1	
Photofrin ^e		>41	
Cisplatin ^f		20.5 ± 0.2	
[FeL ⁺ (cat)NO ₃] ^{b, g}	6.2 ± 0.1	>100	

^a Uptake of iron inside the HeLa cell measured by ICPOES.

^b The IC₅₀ after visible light irradiation (400–700 nm, 10 J cm⁻²).

^c The IC₅₀ values are 24.4(±0.4) μM for **2** and >100 μM for **1** in red light of 600–720 nm (100 J cm⁻²). The IC₅₀ values are >100 μM for the ligands HBHA and pydpa in light of 400–700 nm.

^d Value taken from reference 43, phqpy = 2,2':6,2'':6'':2''':6''':2'''' phenylquinquepyridine.

^e Value taken from reference 44.

^f Ref. [43].

^g Ref. [20].

3.5. DCFDA assay

A 2',7'-dichlorodihydrofluorescein diacetate (DCFDA) assay was carried out to study the mechanistic aspects of the cell death in HeLa cells (Fig. 5). DCFDA is a cell permeable fluorogenic probe which on oxidation by ROS forms 2',7'-dichlorofluorescein (DCF), having an emission maximum at 528 nm. The DCF fluorescence was detected and quantified from fluorescence-activated cell sorting (FACS) analysis. HeLa cells treated with complex **2** (20 μM) and DCFDA in the dark did not show any increase in green fluorescence. However, upon exposure to visible light (400–700 nm) there was a shift in green fluorescence, indicating ROS generation.

3.6. Cellular imaging

The pyrene-based fluorescence of complex **2** was utilized to study the cellular uptake and localization of the complex in HeLa cells. The cells were incubated with complex **2** in the dark for 2 and 4 h. Fluorescence microscopy images showed significant uptake of the complex in the cytosol and some in the nucleus of the cells after 2 h, as was evident by the co-localization of **2** with propidium iodide (PI) which stains the nucleus (Fig. 6). Interestingly, the maximum retention of the complex was observed in the cytosol rather than in the nucleus. After 4 h of incubation, the complex was retained in the cytosol. This observation is important because the PDT drug Photofrin[®] is known for cytosolic

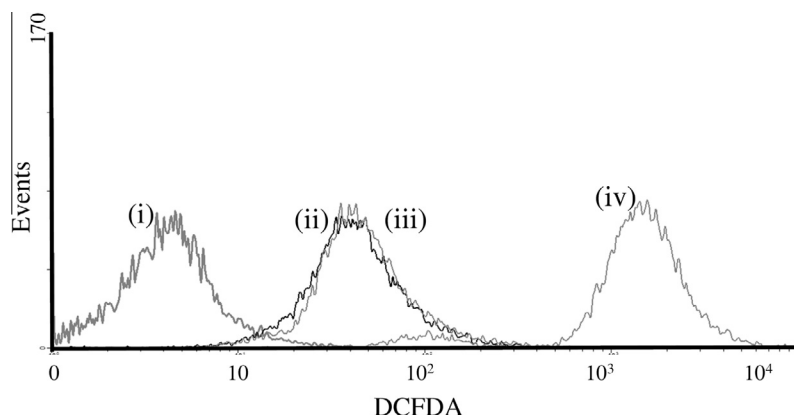


Fig. 5. The shift in the fluorescence band position compared to only the cells under different conditions in a DCFDA assay measured by FACS analysis: (i) only cells, (ii) cells + DCFDA, (iii) cells + complex **2** (in dark), and (iv) cells + complex **2** (on light activation).

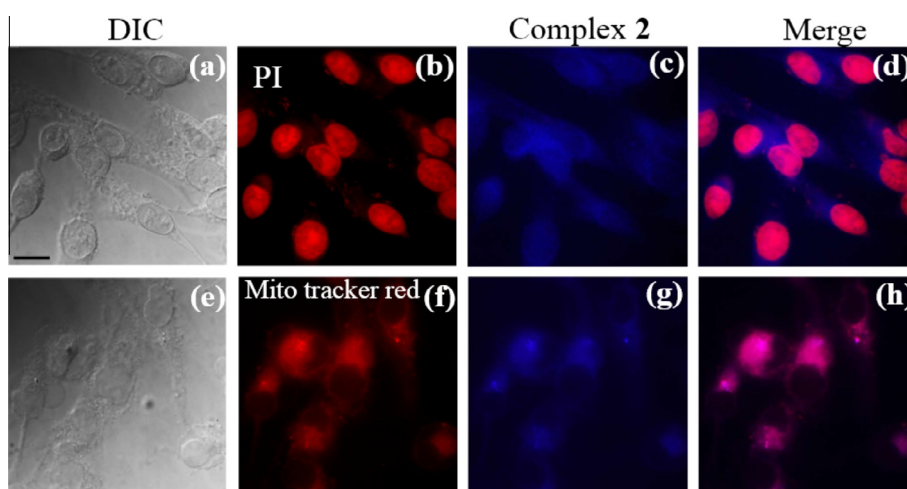


Fig. 6. Fluorescence microscopy images of complex **2** in HeLa cells recorded after 4 h incubation using propidium iodide (PI) and Mito tracker deep red as staining agents for the nucleus and mitochondria, respectively: panels (a) and (e) correspond to bright field images (differential interference contrast); panels (b) and (f) correspond to PI and Mito tracker deep red; panels (c) and (g) correspond to fluorescence of complex **2** and panels (d) and (h) correspond to the merge images. Scale bar corresponds to 0.8 μm . (Color Online.)

localization, particularly in the mitochondria [1]. With the complex accumulating in the cytoplasm, we explored whether the complex was specifically targeting any cellular organelle. For that we carried out dual staining experiments using mitotracker deep red (MTR), which specifically stains mitochondria. The experiment showed complex **2** localizing into the mitochondria in 4 h, as is visible from the merged image shown in panel (h) of Fig. 6. This observation is of significance considering that mitochondria plays a key role in mediating the intrinsic pathway of apoptosis. Thus any changes in the cancer cells leading to protection from apoptosis could be readily targeted using mitochondria specific anticancer agents.

3.7. Iron uptake measurements

Cellular uptake of **1** and **2** in the HeLa cells was quantified by inductively coupled plasma optical emission spectroscopy (ICP-OES). The total iron content in the cell lysate was estimated after incubating the cells with complexes **1** and **2** (20 μM) for 4 h and compared with untreated cells. There was a threefold increase for complex **2**, while a twofold increase was observed for complex **1** for the iron content in the cells. The iron uptake values in the

HeLa cells were 1.97 and 2.79 ng mg^{-1} of protein for **1** and **2**, respectively. The higher uptake of complex **2** could be due to lipophilicity, which is associated with the hydrophobic pyrene moiety.

3.8. DNA binding and cleavage properties

With the knowledge of the nuclear and mitochondrial localization of complex **2**, we were interested to study its DNA binding and DNA cleavage activity, considering that nuclear and mitochondrial DNA could be the potential target of the complex for cellular activity. The binding propensity of complexes **1** and **2** to calf-thymus (ct) DNA was studied using UV-Vis titration, DNA melting and viscometric methods. The equilibrium ct-DNA binding constant (K_b) values of the complexes were obtained from the UV-Vis absorption experiments by monitoring the change in the absorption intensity of the ligand centred band of the complexes near 270 nm [37]. A significant hypochromicity along with a minor bathochromic shift of the band was observed, suggesting a groove binding nature of the complexes to ct-DNA. The K_b values of 2.6×10^5 and $6.4 \times 10^5 \text{ M}^{-1}$ for **1** and **2** indicate their high ct-DNA binding strengths. Viscometric titration experiments were done to determine the relative specific viscosity of ct-DNA on binding to the

complexes. The relative specific viscosity (η/η_0) of DNA gives a measure of the increase in the contour length associated with the separation of DNA base pairs caused by intercalation. A DNA intercalator like ethidium bromide (EB) significantly increases the viscosity of the ct-DNA solution (η and η_0 are the specific viscosities of DNA in the presence and absence of the complex respectively). In contrast, groove or surface binding induces only minor changes in the effective length of DNA, causing smaller changes in the relative viscosity of the DNA solution [45]. The viscometric titration plot of $(\eta/\eta_0)^{1/3}$ versus $[\text{complex}]/[\text{ct-DNA}]$ ratio indicates only a partial intercalative mode of binding of complex **2** to ct-DNA (Fig. 7). The binding interactions were also studied by DNA melting experiments in a phosphate buffer of pH 6.8 (Fig. 8). The shift in the DNA melting temperature (ΔT_m) of 4.0 °C for **2** suggests groove binding or even a partial intercalative mode of binding of this complex to ct-DNA due to the presence of a planar pyrenyl moiety. The DNA intercalator EB gave a ΔT_m value of 13.0 °C under similar experimental conditions.

The chemical nuclease activity of the complexes was studied in the presence of hydrogen peroxide (H_2O_2 , 200 μM) as an oxidizing agent and 3-mercaptopropionic acid (MPA, 1.0 mM) as a reducing agent using supercoiled (SC) pUC19 DNA (0.2 μg , 30 μM) in 50 mM Tris-HCl/50 mM NaCl buffer (pH 7.2). The extent of DNA cleavage was estimated from the gel electrophoresis data. The redox-active iron(III) complexes showed only moderate chemical nuclease activity in the presence of MPA, possibly due to formation of reactive iron(II) species which can generate hydroxyl radicals by activating molecular oxygen, as is known for iron containing anticancer agents, viz. bleomycins [46]. Control experiments using the dipicolylamine ligand, hydroxamic acid, H_2O_2 and MPA alone did not show any apparent cleavage of DNA under similar experimental conditions.

The photo-induced DNA cleavage activity of the complexes was studied using supercoiled (SC) pUC19 DNA upon exposure to red light of 647 nm from a CW (continuous-wave) Ar-Kr mixed gas ion laser (Table 5, Fig. 9). Complex **2** showed efficient photocleavage of SC DNA. A 50 μM solution of this complex showed essentially complete cleavage of the plasmid SC DNA to its nicked circular (NC) form upon irradiation with red light of 647 nm for 2 h. The complexes did not show any significant DNA cleavage activity when incubated in the dark, thus ruling out any possibility of hydrolytic cleavage of DNA. Control experiments with the metal salt or the dipicolylamine ligands showed no apparent photocleavage of DNA.

The mechanistic aspects of the DNA photocleavage reactions were studied using different additives, viz. 1,4-diazabicyclo[2.2.2]octane (DABCO, 1.0 mM), 2,2,6,6-tetramethylpiperidine

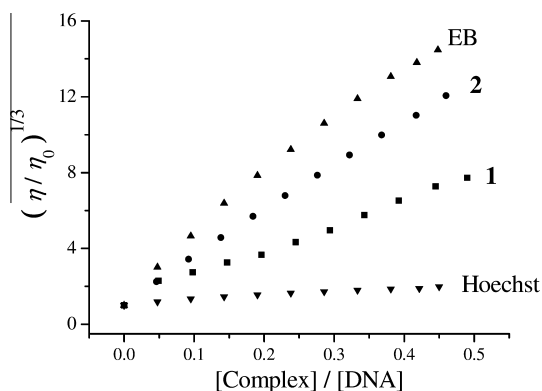


Fig. 7. Plots showing the effect of addition of an increasing quantity of **1** or **2**, ethidium bromide (EB) and Hoechst dye on the relative viscosity of ct-DNA (140 μM) at 37.0 °C (EB, ethidium bromide).

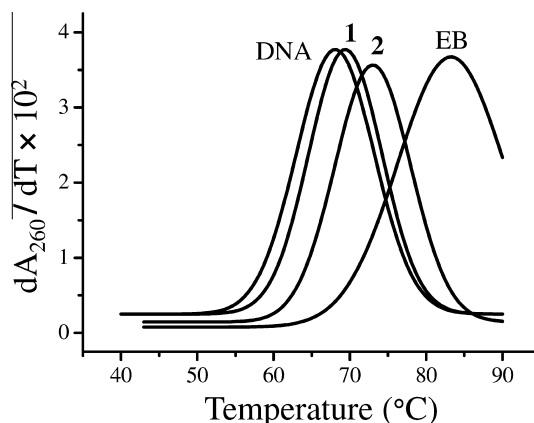


Fig. 8. DNA melting plots of 150 μM ct-DNA alone and in the presence of **1**, **2** and EB in phosphate buffer (pH 6.8) with a $[\text{DNA}]/[\text{complex}]$ ratio of 10:1.

Table 5

Selected SC DNA (pUC19, 0.2 μg) cleavage data^{a,b} for complexes **1** and **2** along with the ligands under different experimental conditions (NC, nicked circular DNA).

Experimental condition	% NC
DNA control ^a	2
DNA + pydpa ^a	5
DNA + HBHA ^a	2
DNA + 1 ^b	4
DNA + 2 ^b	3
DNA + 1 + H_2O_2 ^b	8
DNA + 2 + H_2O_2 ^b	10
DNA + 1 + MPA ^b	25
DNA + 2 + MPA ^b	33
DNA + 1 ^a	15
DNA + 2 ^a	90

^a In red light of 647 nm.

^b In the dark.

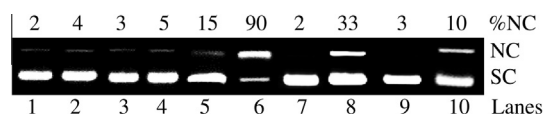


Fig. 9. Cleavage of SC pUC19 DNA (0.2 μg , 30 μM) by $[\text{Fe}(\text{BHA})(\text{L})\text{Cl}]\text{Cl}$ (50 μM , L = phdpa, **1**; pydpa, **2**) and the ligands in 50 mM Tris-HCl/NaCl buffer (pH 7.2) containing 10% DMF on irradiation with red light of 647 nm (2 h exposure) (lanes 1–6) and in the dark (lanes 7–10): lane 1, DNA control; lane 2, DNA + FeCl_3 ; lane 3, DNA + phdpa; lane 4, DNA + pydpa; lane 5, DNA + **1**; lane 6, DNA + **2**; lane 7, DNA + MPA; lane 8, DNA + MPA + **2**; lane 9, DNA + H_2O_2 ; lane 10, DNA + H_2O_2 + **2**.

(TEMP, 1.0 mM), sodium azide (NaN_3 , 1.0 mM) and L-histidine (1.0 mM) as singlet oxygen quenchers, DMSO (4 μL), KI (1.0 mM) and catalase (4 units) as hydroxyl radical scavengers, and superoxide dismutase (SOD, 4 units) as a superoxide radical scavenger. An inhibition of the DNA photocleavage by ~70% was observed in the presence of the hydroxyl radical scavengers, while the singlet oxygen quenchers showed no apparent effect on the DNA cleavage activity (Fig. 10). The photo-induced DNA cleavage activity seems to be metal-assisted, forming hydroxyl radicals involving the LMCT band in the visible region. The data indicate a photo-redox mechanistic pathway to be operative, in which reduction of Fe(III) on photo-activation of the LMCT band could form a charge separated $\text{Fe}^{2+}\text{-L}^+$ (BHA ligand radical cation) species that reduces O_2 to O_2^- by the reactive Fe^{2+} ion, with subsequent formation of hydroxyl radicals (HO^\bullet) in the reaction: $3\text{O}_2^- + 2\text{H}^+ \rightarrow \text{HO}^\bullet + \text{HO}^- + 2\text{O}_2$ [47]. Such a mechanistic pathway is known for iron(III) complexes

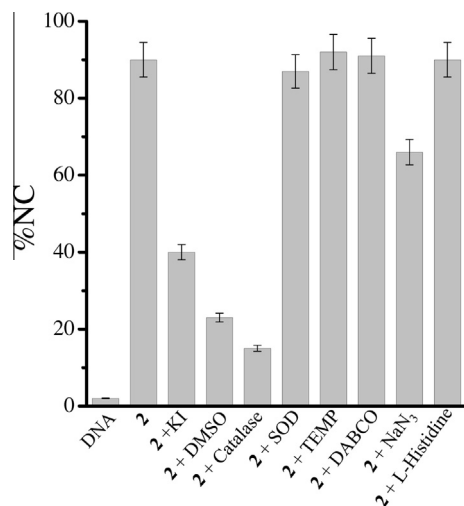


Fig. 10. Bar diagram showing the formation of the %NC DNA in the presence of complex **2** (50 μ M) and various additives in 10% DMF/Tris-HCl buffer (50 mM) in red light of 647 nm [TEMP, DABCO, L-histidine, KI of 0.5 mM; DMSO = 4 μ L; SOD, catalase = 4 units].

having phenolate ligands and for chemical nuclease activity in the dark in the presence of MPA [48]. This pathway is facilitated in the presence of a quasi-reversible redox couple near 0.1 V vs. SCE. The ROS involved in the cellular damage could be reactive hydroxyl species, as evidenced from this mechanistic study.

4. Conclusions

An iron(III) benzhydroxamate complex of a dipicolylamine ligand having a pendant pyrenyl moiety showed remarkable red light-induced photo-cytotoxicity in HeLa cells with desirable mitochondrial localization, along with nuclear uptake. The PDT activity is due to the presence of an intense LMCT band involving the benzhydroxamate-iron(III) moiety with a tail that extended up to the near-IR region. Photo-activation in red light generates cytotoxic hydroxyl radical species, probably involving the LMCT band. The complexes are non-toxic in the dark. The results are of significance considering that metal-based PDT agents showing similar mitochondrial localization and photocytotoxicity within the therapeutic spectral window of 600–800 nm are important in PDT. The results are expected to presage further development of the chemistry of iron-based PDT agents for targeted therapeutic applications.

Acknowledgements

A.R.C. thanks the Department of Science and Technology (DST), Government of India, and the Council of Scientific and Industrial Research (CSIR, New Delhi) for financial support (SR/S5/MBD-02/2007; CSIR/01 (2559)/12/EMR-II/2012) and DST for the J.C. Bose national fellowship. I.K. thanks CSIR for a fellowship. We are thankful to the Alexander von Humboldt Foundation (Germany) for donation of an electrochemical system and DST for a CCD diffractometer facility.

Appendix A. Supplementary data

CCDC 912568 contains the supplementary crystallographic data for this paper. These data can be obtained free of charge via <http://www.ccdc.cam.ac.uk/conts/retrieving.html>, or from the Cambridge Crystallographic Data Centre, 12 Union Road, Cambridge CB2 1EZ,

UK; fax: (+44) 1223-336-033; or e-mail: deposit@ccdc.cam.ac.uk. Supplementary data associated with this article can be found in the online version, at <http://dx.doi.org/10.1016/j.poly.2014.02.018>.

References

- [1] R. Bonnett, *Chemical Aspects of Photodynamic Therapy*, Gordon & Breach, London, UK, 2000.
- [2] J.F. Lovell, T.W.B. Liu, J. Chen, G. Zheng, *Chem. Rev.* 110 (2010) 2839.
- [3] J.P. Celli, B.Q. Spring, I. Rizvi, C.L. Evans, K.S. Samkoe, S. Verma, B.W. Pogue, T. Hasan, *Chem. Rev.* 110 (2010) 2795.
- [4] M. Ethirajan, Y. Chen, P. Joshi, R.K. Pandey, *Chem. Soc. Rev.* 40 (2011) 340.
- [5] P. Couleaud, V. Morosini, C. Frochot, S. Richeter, L. Raehm, J.-O. Durand, *Nanoscale* 2 (2010) 1083.
- [6] A. Kamkaew, S.H. Lim, H.B. Lee, L.V. Kiew, L.Y. Chung, K. Burgess, *Chem. Soc. Rev.* 42 (2013) 77.
- [7] P. Agostinis, K. Berg, K.A. Cengel, T.H. Foster, A.W. Girotti, S.O. Gollnick, S.M. Hahn, M.R. Hamblin, A. Juzeniene, D. Kessel, M. Korbelik, J. Moan, P. Mroz, D. Nowis, J. Piette, B.C. Wilson, J. Golab, *CA Cancer J. Clin.* 61 (2011) 250.
- [8] K. Szaciłowski, W. Macyk, A. Drzewiecka-Matuszek, M. Brindell, G. Stochel, *Chem. Rev.* 105 (2005) 2647.
- [9] A.B. Ormond, H.S. Freeman, *Materials* 6 (2013) 817.
- [10] S.I. Moriwaki, J. Misawa, Y. Yoshinari, I. Yamada, M. Takigawa, Y. Tokura, *Photodermatol. Photoimmunol. Photomed.* 17 (2001) 241.
- [11] C.J. Burrows, J.G. Muller, *Chem. Rev.* 98 (1998) 1109.
- [12] (a) N.J. Farrer, L. Salassa, P.J. Sadler, *Dalton Trans.* (2009) 10690; (b) P.K. Sasmal, C.N. Streu, E. Meggers, *Chem. Commun.* 49 (2013) 1581; (c) O.J. Stacey, S.J.A. Pope, *RSC Adv.* 3 (2013) 25550.
- [13] F.S. Mackay, J.A. Woods, P. Heringová, J. Kašpárková, A.M. Pizarro, S.A. Moggach, S. Parsons, V. Brabec, P.J. Sadler, *Proc. Nat. Acad. Sci. USA* 104 (2007) 20743.
- [14] (a) N.L. Fry, P.K. Mascharak, *Acc. Chem. Res.* 44 (2011) 289; (b) J. Wang, J. Newman Jr., S.L.H. Higgins, K.M. Brewer, B.S.J. Winkel, K.J. Brewer, *Angew. Chem., Int. Ed.* 52 (2013) 1262.
- [15] (a) J. Liu, Z. Cao, Y. Lu, *Chem. Rev.* 109 (2009) 1948; (b) S.L.H. Higgins, A.J. Tucker, B.S.J. Winkel, K.J. Brewer, *Chem. Commun.* 48 (2012) 67.
- [16] B. Maity, A.R. Chakravarty, *Indian J. Chem., Sect. A* 51 (2012) 69.
- [17] (a) P.K. Sasmal, S. Saha, R. Majumdar, R.R. Dighe, A.R. Chakravarty, *Chem. Commun.* (2009) 1703; (b) T.K. Goswami, B.V.S.K. Chakravarthi, M. Roy, A.A. Karande, A.R. Chakravarty, *Inorg. Chem.* 50 (2011) 8452.
- [18] (a) S. Banerjee, A. Hussain, P. Prasad, I. Khan, B. Banik, P. Kondaiah, A.R. Chakravarty, *Eur. J. Inorg. Chem.* (2012) 3899; (b) S. Dhar, D. Senapati, P.A.N. Reddy, P.K. Das, A.R. Chakravarty, *Chem. Commun.* (2003) 2452.
- [20] P. Prasad, P.K. Sasmal, I. Khan, P. Kondaiah, A.R. Chakravarty, *Inorg. Chim. Acta* 372 (2011) 79.
- [20] U. Basu, I. Khan, A. Hussain, P. Kondaiah, A.R. Chakravarty, *Angew. Chem., Int. Ed.* 51 (2012) 2658.
- [21] P.U. Maheswari, S. Roy, H. den Dulk, S. Barends, G. vanWeszel, B. Kozlevcar, P. Gamez, J. Reedijk, *J. Am. Chem. Soc.* 128 (2006) 710.
- [22] K. Visvaganesan, R. Mayilmurugan, E. Suresh, M. Palaniandavar, *Inorg. Chem.* 46 (2007) 10294.
- [23] (a) S. Fulda, L. Galluzzi, G. Kroemer, *Nat. Rev. Drug Discov.* 9 (2010) 447; (b) J.S. Armstrong, *Brit. J. Pharmacol.* 147 (2006) 239.
- [24] (a) S. Marrachea, S. Dhar, *Proc. Natl. Acad. Sci. USA* 104 (2012) 16288; (b) S. Marrachea, S. Tundup, D.A. Harn, S. Dhar, *ACS Nano* 7 (2013) 7392.
- [25] C.E. Wenner, *J. Cell. Physiol.* 227 (2011) 450.
- [26] D. Rojas, A.M. García, A. Vega, Y. Moreno, D. Venegas-Yazigi, M.T. Garland, J. Manzur, *Inorg. Chem.* 43 (2004) 6324.
- [27] L.A. Mullice, R.H. Laye, L.P. Harding, N.J. Buurma, S.J.A. Pope, *New J. Chem.* 32 (2008) 2140.
- [28] N. Walker, D. Stuart, *Acta Crystallogr., Sect. A* 39 (1983) 158.
- [29] G.M. Sheldrick, *SHELX-97*, Programs for crystal structure solution and refinement, University of Göttingen, Göttingen, Germany, 1997.
- [30] C.K. Johnson, ORTEP, Report ORNL-5138; Oak Ridge National Laboratory: Oak Ridge, TN, 1976.
- [31] L. Zhang, W. Liu, K.K. Szumilinski, J. Lew, *Proc. Natl. Acad. Sci. USA* 109 (2012) 20041.
- [32] T. Esteves, F. Marques, A. Paulo, J. Rino, P. Nanda, C.J. Smith, I. Santos, *J. Biol. Inorg. Chem.* 16 (2011) 1141.
- [33] T. Takanashi, Y. Ogura, H. Taguchi, M. Hashizoe, Y. Honda, *Invest. Ophthalmol. Vis. Sci.* 38 (1997) 2721.
- [34] S. Banerjee, P. Prasad, A. Hussain, I. Khan, P. Kondaiah, A.R. Chakravarty, *Chem. Commun.* 48 (2012) 7702.
- [35] S.P. Foxon, C. Metcalfe, H. Adams, M. Webb, J.A. Thomas, *Inorg. Chem.* 46 (2007) 409.
- [36] M.E. Reichmann, S.A. Rice, C.A. Thomas, P. Doty, *J. Am. Chem. Soc.* 76 (1954) 3047.
- [37] (a) J.D. McGhee, P.H. Von Hippel, *J. Mol. Biol.* 86 (1974) 469; (b) M.T. Carter, M. Rodriguez, A.J. Bard, *J. Am. Chem. Soc.* 111 (1989) 8901.
- [38] S. Saha, R. Majumdar, M. Roy, R.R. Dighe, A.R. Chakravarty, *Inorg. Chem.* 48 (2009) 2652.

- [39] J. Bernadou, G. Pratviel, F. Bennis, M. Girardet, B. Meunier, *Biochemistry* 28 (1989) 7268.
- [40] E. Galardon, M. Selkti, P. Roussel, A. Tomas, I. Artaud, *Dalton Trans.* (2008) 6415.
- [41] T.A. Sherstneva, K.P. Birin, V.V. Arslanov, *Prot. Met.* 49 (2013) 72.
- [42] K. Nakamoto, *Infrared and Raman Spectra of Inorganic and Coordination Compounds*, John Wiley & Sons, New York, 1997.
- [43] E.L.M. Wong, G.S. Fang, C.M. Chi, N. Zhu, *Chem. Commun.* (2005) 4578.
- [44] E. Delaey, F. van Laar, D. De Vos, A. Kamuhabwa, P. Jacobs, P. de Witte, J. *Photochem. Photobiol.*, B 55 (2000) 27.
- [45] K.E. Reinert, *Biochim. Biophys. Acta* 319 (1973) 135.
- [46] R.M. Burger, *Chem. Rev.* 98 (1998) 1153.
- [47] T.A. van den Berg, B.L. Feringa, G. Roelfes, *Chem. Commun.* (2007) 180.
- [48] A. Mukherjee, S. Dhar, M. Nethaji, A.R. Chakravarty, *Dalton Trans.* (2005) 349.